RESEARCH ARTICLE

Acyclic Cucurbit[n]uril Type Receptors: Aromatic Wall Extension Enhances Binding Affinity, Delivers Helical Chirality, and Enables Fluorescence Sensing

Steven Murkli,[a] Jared Klemm,[a] David King,[a] Peter Y. Zavalij,[a] and Lyle Isaacs*[a]

[a] Mr. Steven Murkli, Mr. Jared Klemm, Mr. David King, Dr. Peter Y. Zavalij, Prof. Dr. Lyle Isaacs
Department of Chemistry and Biochemistry
University of Maryland, College Park, MD 20742
United States
LIsaacs@umd.edu

Supporting information for this article is given via a link at the end of the document.

Abstract: We report the linear extension from **M1** to **M2** to anthracene walled **M3** which adopts a helical conformation (x-ray) to avoid unfavorable interactions between sidewalls. **M3** is water soluble (≈ 30 mM) and displays enhanced optical properties (ε = 1.28 x 10^5 M^{-1} cm^{-1}, λ_{max} = 370 nm) relative to **M2**. The binding properties of **M3** toward guests **1**-**29** were examined by ^{1}H NMR and ITC. The **M3**•guest complexes are stronger than the analogous complexes of **M2** and **M1.** The enhanced binding of **M3** toward neuromuscular blockers **25**, **27**-**29** suggests that **M3** holds significant promise as an *in vivo* reversal agent. The changes in fluorescence observed for **M3**•guest complexes are a function of the relative orientation of the anthracene sidewalls, [guest], K_a, and guest electronics which rendered **M3** a superb component of a fluorescence sensing array. The work establishes **M3** as a next generation sequestering agent and a versatile component of fluorescence sensors.

Introduction

Molecular recognition events constitute the essential element of life processes that control biosynthesis, translocation, self versus non-self recognition, and self-regulation. Within the realm of supramolecular chemistry, scientists have sought to understand the fundamentals of non-covalent interactions[1] in organic solvents and aqueous solution and to use this knowledge to create systems that display useful functions including sensing ensembles,[2] molecular machines,[3] non-covalent polymers,[4] separations phases,[5] and (targeted) drug delivery. The preparation, study, and application of new classes of macrocyclic receptors (e.g. molecular containers) occupies a central role in the field of supramolecular chemistry because the pre-organization inherent to macrocyclic scaffolds generally results in high affinity and selectivity. Some of the most popular classes of macrocyclic receptors include the crown ethers,[1c] cryptands,[1b] cyclodextrins,[6] calixarenes,[7] cyclophanes,[1a, 3a, 8] cavitands,[9] pillararenes,[10] as well as cages self-assembled by H-bonding, the hydrophobic effect, and metal-ligand interactions.[9c, 11] Macrocycles are at the heart of solutions to societally important problems including the formulation of insoluble drugs,[6] the household product Febreeze™,[12] glucose monitors,[13] sequestrants for nuclear waste ions,[14] and the removal of contaminants from water sources.[15] Amongst these molecular containers, cucurbit[n]urils (CB[n], Figure 1)[16] have distinguished themselves due to their ability to form high affinity CB[n]•guest complexes in highly selective and stimuli responsive processes in aqueous solution.[17] Accordingly, macrocyclic CB[n] and their derivatives have been extensively investigated as components of sensing ensembles,[18] molecular machines,[19] in pharmaceutical applications,[20] as catalysts,[21] and are even beginning to appear in commercial deodorizing products.[22]

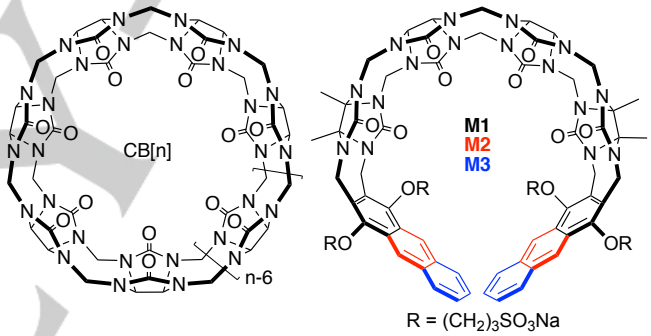

Figure 1. Structures of CB[n], **M1**, **M2**, and **M3.**

In the past decade, we and others have been interested in the preparation and molecular recognition properties of acyclic CB[n]-type receptors (e.g. **M1** and **M2**, Figure 1).[23] **M1** and **M2** are composed of a central glycoluril tetramer which imparts an overall C-shape[24] and hydrophobic cation binding properties, two aromatic sidewalls which allow **M1** and **M2** to engage in π–π interactions with aromatic guests, and four SO_3^- groups that electrostatically enhance binding affinity and deliver high aqueous solubility. By virtue of their pre-organized polycyclic framework which contains only limited degrees of freedom (e.g. in-plane flexing and out-of-plane skewing), acyclic CB[n] display high binding affinities toward hydrophobic ammonium ion guests that are typical of macrocyclic CB[n]. Accordingly, we have explored the use of **M1**, **M2**, and derivatives as solubilizing excipients for insoluble drugs for *in vivo* delivery,[25] as *in vivo* reversal agents for neuromuscular blocking agents and drugs of abuse,[26] and as components of sensing arrays for drugs.[27] Because acyclic CB[n] are more straightforward to modify synthetically than macrocyclic CB[n], we have developed medicinal chemistry type structure-binding relationships in the acyclic CB[n]-type receptor series. For example, we have studied variants based on glycoluril monomer – tetramer,[28] different sidearm-solubilizing group combinations,[29] covalent capping strategies,[30] and different

aromatic sidewalls (e.g. functionalized benzene, naphthalene, and triptycene).[31] To date, however, the **M1** host remains our most general purpose receptor and its variant **M2**, prepared conceptually by linear in-plane extension of aromatic walls, remains our most potent receptor for *in vivo* sequestration applications. In this paper, we further explore the linear in-plane extension of the aromatic walls to deliver the anthracene walled acyclic CB[n]-type receptor **M3** as a means to further enhance binding affinity and to imbue the receptor with improved optical properties for sensing applications.

Results and Discussion

This results and discussion section is subdivided as follows. First, we describe the design, synthesis and characterization of **M3** by spectroscopic and crystallographic means. Next, we qualitatively study the behavior of **M3** and **M3**•guest complexation *via* (variable temperature) ^{1}H NMR. Subsequently, isothermal titration calorimetry (ITC) is used to determine the thermodynamic parameters of binding of **M3** toward a panel of typical guests for (acyclic) CB[n] (**1** – **29**) followed by a discussion of the trends in the binding data relative to **M2** as comparator. Finally, we demonstrate the high potential of the anthracene walled **M3** as a component of sensor arrays for hydrophobic cations.

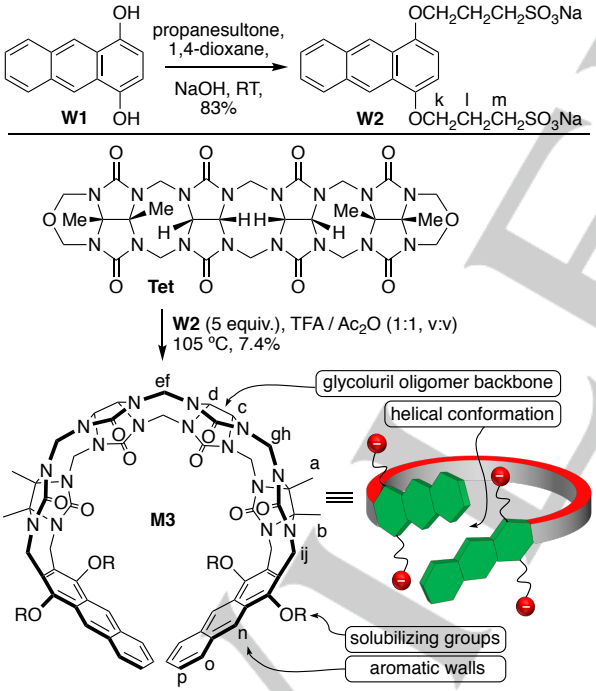

Scheme 1. Synthesis of anthracene walled host **M3** and an illustration of the helical conformation that it adopts. R = $(CH_2)_3SO_3Na$

Design, synthesis, and characterization of Acyclic CB[n]-Type Host M3. Previously, we have found that extension of the aromatic sidewalls from benzene walled **M1** to naphthalene walled **M2** enhances the binding affinity toward larger hydrophobic cationic guests.[26c, 31] Based on x-ray crystallography, we observed that the longer naphthalene sidewalls undergo edge-to face π–π interactions which expands the size of the hydrophobic cavity of **M2** relative to **M1**. Previously, our attempt to further increase cavity size and binding affinity by using triptycene sidewalls was thwarted by the crystallographically observed self-folding of one blade of the triptycene sidewall into its own cavity.[32] Accordingly, in this paper we decided to investigate the linear extension of naphthalene walled **M2** to anthracene walled **M3** with the hypothesis that the rigid sidewalls would either adopt a helically chiral conformation or buttress each other and thereby further expand the size of the cavity and the number of cavity bound water molecules which is known in the CB[n] family to be a major determinant of binding affinity.[33]

The synthesis of anthracene walled host **M3** follows our building block approach based on double electrophilic aromatic substitution reactions between glycoluril bis(cyclic ethers) and activated dialkoxy aromatic sidewalls.[23a] We prepared 1,4-dihydroxynaphthalene **W1** (Scheme 1) by modifications of the literature procedures on the 33 g scale.[34] To install the water solubilizing sulfonate groups, **W1** was reacted with 1,3-propanesultone under basic conditions in 1,4-dioxane to deliver **W2** in 83% yield. Subsequently, methylene bridged glycoluril tetramer (**Tet**) was allowed to react with **W2** under acidic conditions (TFA / Ac_2O, 1:1) at 110 °C in a sealed tube to deliver crude **M3** (Scheme 1) after precipitation with acetone. Purification of **M3** was achieved by repeated washing of the crude material with MeOH, followed by size exclusion chromatography (Sephadex G25) using H_2O as eluent to afford **M3** in 7.4% yield. Host **M3** was characterized by ^{1}H NMR, ^{13}C NMR, IR, and UV/Vis spectroscopy, by electrospray ionization mass spectrometry, and ultimately by single crystal diffraction (*vide infra*). Figure 2f and 2g show the ^{1}H NMR spectra recorded for **M3** at room temperature in D_2O and DMSO-d_6, respectively. Clearly, **M3** undergoes self-association in water as evidenced by the broadening of the resonances belonging to the anthracene walls (H_n, H_o, and H_p) as well as the methyl groups (H_a and H_b) on the convex face of **M3**. In DMSO-d_6, however, sharp resonances are observed for **M3** and the number and multiplicity of the resonances are consistent with time averaged C_{2v}-symmetry depicted in the line-bond drawing of **M3** given in Scheme 1. The ^{13}C NMR spectrum of **M3** displays 20 of the 21 expected resonances for C_{2v}-symmetric **M3** due to accidental degeneracy of the two CH_3 resonances. Scheme 1 also shows a schematic representation of a helical conformation of **M3** that could occur due to steric clashes between the anthracene walls.[35] The presented ^{1}H and ^{13}C NMR data is also consistent with a rapidly equilibrating mixture of both senses of helical chirality. In order to gauge the self-association and dynamic properties of **M3** in water we first performed a dilution experiment monitored by ^{1}H NMR (Figure S5). The change in chemical shift of H_n, H_o, and H_p of **M3** as a function of concentration (3.1 mM – 0.14 mM) does not fit well to a two-fold self-association model.[36] We also collected variable temperature ^{1}H NMR in D_2O (Figure 2a-f) over the 298 – 348 K range and observed the sharpening or coalescence of the resonances for **M3** ultimately delivering a spectrum indicative of time averaged C_{2v}-symmetry. Lastly, ESI-MS spectrum of **M3** shows a doubly charged ion at *m/z* 847 which is in accord with value calculated for the $[M - 2Na]^{2-}$ ion. Given the potential to use anthracene walled **M3** as a component of sensing arrays we measured its UV/Vis spectrum (Figure S7) in water and

determined its molar extinction coefficient (ε = 1.28 × 10^5 M^{-1} cm^{-1}) at λ_{max} = 370 nm. Both the ε and λ_{max} values of **M3** are larger than for **M2** (ε = 1.66 × 10^4 M^{-1} cm^{-1}; λ_{max} = 282), the 1,8-substituted isomer of **M2** (ε = 1.58 × 10^4 M^{-1} cm^{-1}; λ_{max} = 301 nm), and triptycene walled glycoluril tetramer (ε = 6.6 × 10^4 M^{-1} cm^{-1}; λ_{max} = 214 nm) which enhances the potential of **M3** in sensing applications.[27c, 32] The inherent solubility of **M3** in water (≈ 30 mM) was sufficient to enable studies of its molecular recognition properties and tease out the impact of the anthracene walls using **M2** as comparator.

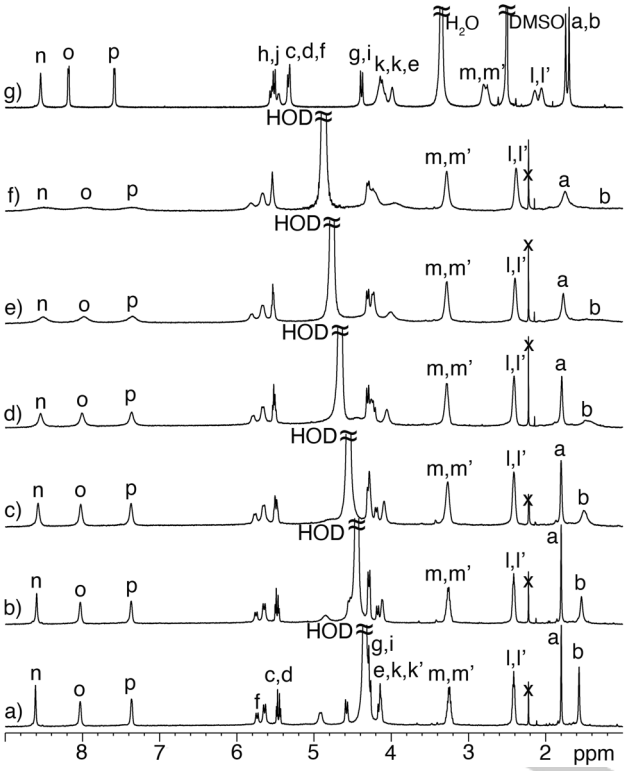

Figure 2. ^{1}H NMR spectra recorded (600 MHz, **M3** (0.5 mM), D_2O) for a) 348 K, b) 338 K, c) 328 K, d) 318 K, e) 308 K, f) 298 K, g) **M3** (0.5 mM) in DMSO. X = acetone (internal standard).

X-ray Crystal Structure of W2 and M3. Figure 3 shows the x-ray crystal structures of **W2** (CCDC 2003752) and uncomplexed **M3** (CCDC 2003754). Figure 3a shows the packing of **W2** in the crystal within the xy-plane. Two different pairs of anthracene rings can be identified. The first pair (labelled @) assumes an offset π–π stacked geometry with an average interplanar separation of 3.381 Å. The mean interplanar separation between the second pair of anthracenes (labelled $) is 3.481 Å, but they are sufficiently offset from one another that no direct interactions between these rings occur. Instead this pair of anthracenes appears to interact *via* C-H•••π interactions from the $O(CH_2)_3SO_3Na$ arm of one anthracene and the opposing anthracene and vice versa (labelled *); C-H•••π-plane distances: 2.890, 2.878, 2.679 Å). Finally, two pairs of Ar-H groups on the tips of the π–π stacked pair anthracene rings (pair labelled @) undergo C-H•••π interaction (labelled #) with the face of one anthracene ring of the other pair (labelled $, C-H•••π-plane distances = 2.792, 2.941, 2.628, 2.697 Å). These sheets of molecules in the xy-plane point their SO_3^- groups in the z-direction. The sheets of **W2** stack in the z-direction held together by the Na^+ counterions (not shown).

Figure 3b shows the x-ray crystal structure of uncomplexed **M3**. Several features of the geometry of **M3** and its packing in the solid state are noteworthy. Most striking is that the anthracene sidewalls are skewed out of plane with respect to the equator of the glycoluril tetramer backbone; the angle between the mean planes of the anthracene sidewalls amounts to 94.34°. Extension of the aromatic sidewalls from **M1** to **M2** to **M3** requires this out-of-plane skewing to prevent serious steric interactions between the sidewalls and results in an overall helical chirality of **M3** in the solid state. One molecule of isopropanol is included in the cavity of **M3** and forms a H-bond to a ureidyl C=O group on the portal of **M3** (C=O•••H distance: 2.143 Å; O•••O distance: 2.930 Å; C=O•••H-O angle: 155.92°). Two of the $(CH_2)_3SO_3Na$ sidearms partially invade the cavity of **M3** by packing against the face of the opposing anthracene sidewall assisted by CH•••π interactions (marked +). Figure 3b shows that molecules of **M3** form tapes of alternating helical chirality packed along the x-axis assisted by two different types of interactions between the anthracene sidewalls. One pair of anthracenes (marked =) forms an offset π–π stacked geometry with the mean interplanar separation of the anthracene sidewalls of 3.259 Å. The second pair of anthracenes (marked ≈) are roughly coplanar with one other but have a mean interplanar separation of 3.805 Å which is beyond the usual π–π stacking distance. Instead, each anthracene sidewall engages in C-H•••π interactions with the CH_3 and CH_2 groups on the opposing **M3** molecule (CH_2•••π-plane: 2.671 and 2.847 Å; CH_3•••π-plane: 2.621 Å).[37] The overall 4- charge of **M3** is counterbalanced by four sodium ions in the solid state. These sodium ions and associated waters coordinate to the ureidyl C=O portals of **M3** and form bridges between tapes that assemble along the y- and z-axes (not shown).

We also obtained single crystals of the complex between **M3** and (–)-sparteine (CCDC 2003753, Figure 3c,d). In the x-ray crystal structure, there are four molecules of **M3** (A, B, C, D), two molecules of isopropanol, and four fully occupied sparteines and one sparteine with 50% occupancy in the asymmetric unit. All of the sparteines exist in their dicationic forms and assume the *trans* A/B, chair-chair – *trans* C/D, boat-chair conformation in accord with literature precedent.[38] This conformation points the N-H groups in opposite directions rather than converging as is seen in metal complexes of sparteine free base. An enlarged stereoview of the asymmetric unit is given in the Supporting Information (Figure S104). Figure 3c and 3d only show stereoviews of **M3**-A and **M3**-C which are illustrative of the interesting aspects observed. All four molecules of **M3** display helical chirality in the crystal (A and B: M-helicity; C and D: P-helicity). **M3**-A and **M3**-D each contain a sparteine molecule in their cavity; the sparteine inside **M3**-D is completely disordered and accordingly **M3**-D is not discussed in detail. In contrast, **M3**-B and **M3**-C contain one encapsulated isopropanol and one partially encapsulated sparteine; both structures are similar, so we do not discuss **M3**-B in depth. We observe that the angle between the mean planes of the anthracene sidewalls is dependent upon the encapsulated guests. **M3**-A (85.0°) and **M3**-D (80.9°) which fully encapsulate a large sparteine display more acute angles than **M3**-B (96.1) and **M3**-C (93.0°) which fully encapsulate the smaller isopropanol molecule. The framework of **M3** can twist and flex to accommodate the guest. In **M3**-C, the isopropanol forms a

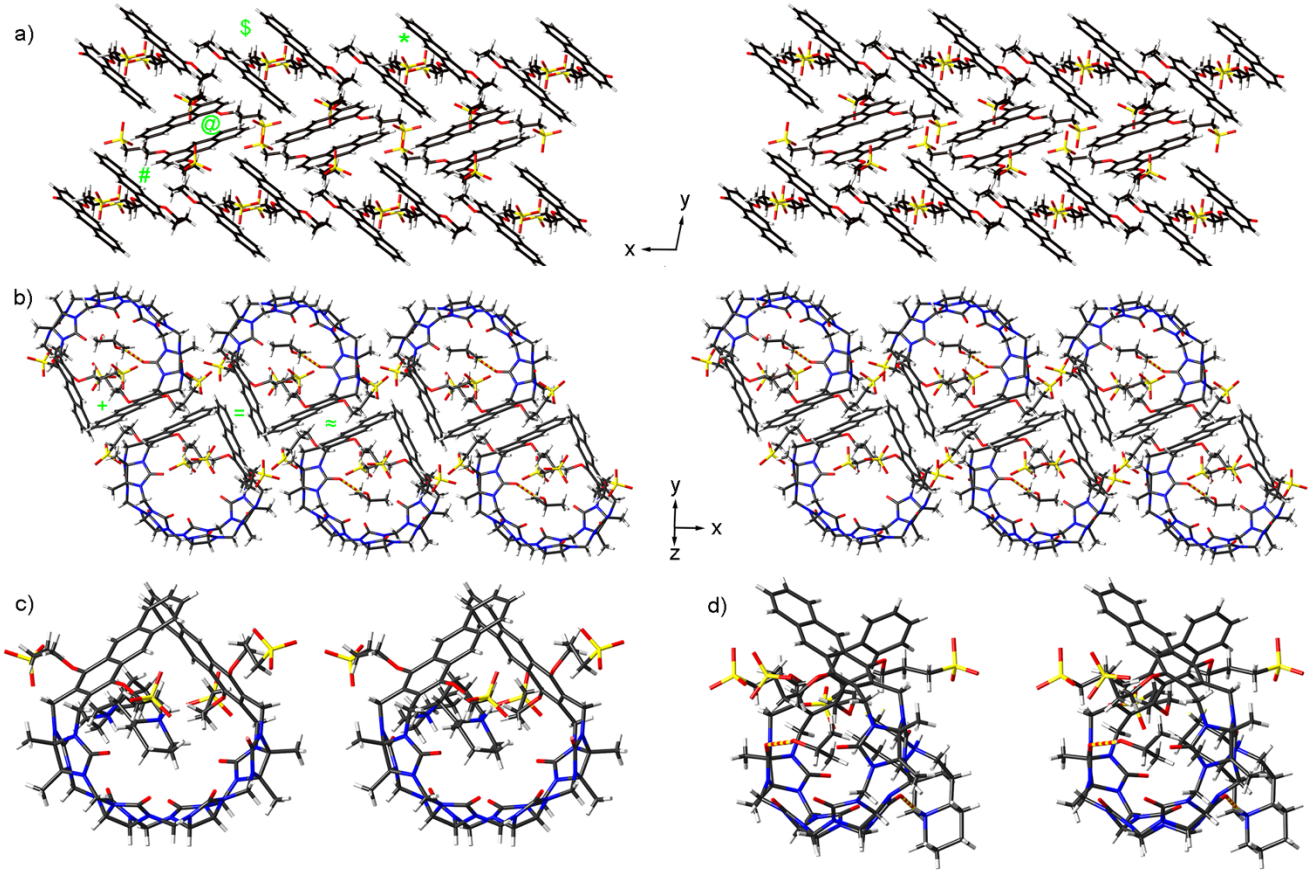

Figure 3. Cross eyed stereoviews the structures of: a) **W2** and b) uncomplexed **M3**. Cross-eyed stereoviews of selected molecules from the crystal structure of **M3•20** complex: c) **20•M3**-A and d) **20•M3**-C with bound isopropanol. Color code: C, gray; H, while; N, blue; O, red; S, yellow; H-bonds, red-yellow striped.

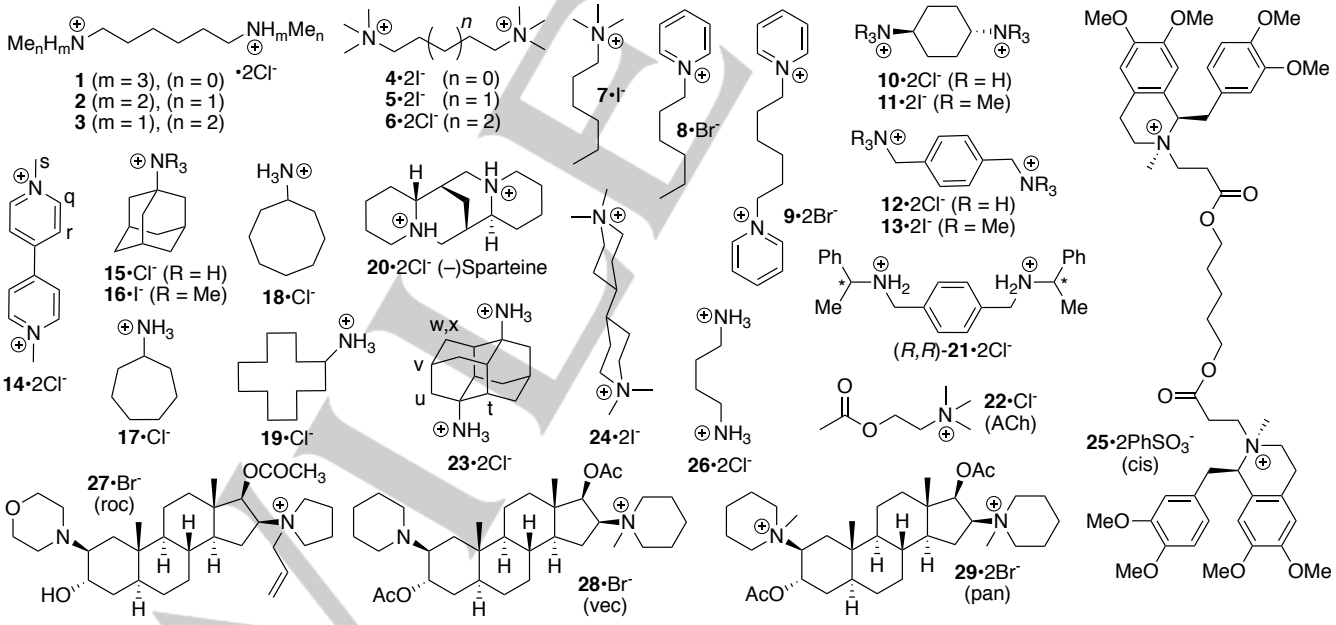

Figure 4. Chemical structures of guests and neuromuscular blocking agents used in this study.

hydrogen bond to the ureidyl C=O of **M3** (HO•••O=C distance: 3.057 Å; OH•••O=C distance: 2.272 Å; O-H•••O=C angle: 156.025˚). As described above, the $O(CH_2)_3SO_3Na$ sidearms of **M3**-C engage in CH•••π interactions (C-H•••π-plane distances: 2.691, 3.254, 3.083, 3.237 Å) with the opposing anthracene sidewall to effectively fill the cavity. The sparteine guest of **M3**-C engages in an N-H•••O=C H-bond with **M3** (N•••O distance: 3.027 Å; N-H•••O distance: 2.064 Å; N-H•••O=C angle 160.395 Å). In addition, the polarized CH and CH_2 groups adjacent to the other ammonium group position themselves nearby the portal O=C groups (C•••O=C distance: 3.042, 3.218, 3.44 Å). In contrast, the larger cavity bound sparteine guest of **M3**-A obviates the need for

its sidearms to engage in CH•••π interactions with the anthracene sidewalls and also does not form an N-H•••O=C H-bond. **M3**-A does, however, display CH•••π contacts (2.972, 2.707 Å) between a polarized N^+-CH_2CH_2 group and the anthracene sidewalls. Overall, the X-ray crystal structures establish that π-extension of the aromatic sidewalls results in helical chirality and that the nature of the guest influences the angular orientation of the anthracene sidewalls with respect to one another.

Qualitative Study of Host•Guest Recognition by ^{1}H NMR Spectroscopy. Having firmly established the structure of **M3** and gained some insight into its propensity for self-association and helical chirality, we turned our attention to the host-guest binding properties of **M3** toward guests **1** – **24** (Figure 4) by ^{1}H NMR spectroscopy. This panel of guests was selected to assess the influence of guest charge (mono versus diammonium, e.g. **6** versus **7**, **8** versus **9**), guest length (e.g. **4** – **6**), methylation state and nature of cationic headgroup (e.g. **1** – **3**, **6**, **9**), guest size (carbon number and width), and guest chirality. Figure 5a shows the ^{1}H NMR spectra recorded for uncomplexed **14** as well as 1:1 and 1:2 mixtures of **M3** with **14**. At a 1:1 ratio of **M3**:**14**, we observe significant upfield shifting for the H_q, H_r, and H_s resonances of guest **14**. Additionally, the resonances belonging to **M3** become nicely resolved upon formation of the **M3•14** complex. Full assignment of glycoluril resonances of **M3•14** in D_2O are detailed in Figure 5b. A comparison of the complexation induced changes in chemical shift of guest **14** in the **M2•14**[39] and **M3•14** complexes (Δδ values: H_q: 0.99 ppm (**M2**), 1.22 ppm (**M3**); H_r: 1.51 ppm (**M2**), 1.63 ppm (**M3**); H_s: 0.25 ppm (**M2**), 0.60 ppm (**M3**)) reveals the stronger anisotropic shielding effect of the larger anthracene π-systems of **M3** compared to the naphthalene sidewalls of **M2**. The upfield shift observed for the $(CH_3)_s$ (0.59 ppm), which should reside near the ureidyl C=O portal of **M3**, suggests that the anthracene sidewalls adopt a helical conformation that brings them in close proximity to the $(CH_3)_s$. In the 1:2 spectra, the signals for free and bound **14** display one set of broadened signals indicating intermediate kinetics of exchange on the chemical shift timescale. Similar qualitative **M3**•guest binding studies were performed for the remainder of the guests (Figures S34 – S57). As expected, the signals corresponding to the hydrophobic domains of each guest exhibits obvious upfield shifting upon complexation due to the shielding effect of the glycoluril cavity as well as the anisotropic shielding effect of the π-surfaces of the anthracene walls of **M3**.

In contrast, Figure 5d-f shows the ^{1}H NMR spectra recorded for the very wide guest **23**, the **M3•23** complex, and a 1:2 mixture of **M3** and **23**. In Figure 5c, we observe separate sharp resonances (H_t, H_u, H_v and H_w) for free guest **23** and the **M3•23** complex which establishes slow kinetics of guest exchange on the chemical shift timescale. Guest **23** exhibits dramatic upfield shifting of the resonances for its diamantane hydrophobic domain (Δδ values: H_t: 1.72 ppm; H_u: 1.73 ppm; H_v: 2.25 ppm; H_w: 2.52 ppm;) indicating inclusion in the **M3** cavity. Previously, we have found that CB[7] and CB[8] form complexes with **23** (CB[7]•**23**: K_a = 2030 M^{-1}; CB[8]•**23**: K_a = (3.3 ± 0.8) × 10^{13} M^{-1}) and that CB[7] does so with fast kinetics of exchange whereas CB[8] displays slow kinetics of exchange.[40] Similarly, the smaller acyclic CB[n] host **M2** displays fast kinetics of guest exchange with **23**. These observations, in accord with the results from x-ray crystallography suggest that **M3** is able to expand the size of its cavity by flexing its methylene bridged glycoluril tetramer backbone to accommodate guests typically observed to bind well to CB[8]. As such, the thermodynamics of guest binding of **M3** may prove to be distinct from previous acyclic CB[n]-type receptors such as **M2**. Chiral and enantiomerically pure guests (–)-sparteine (**20**) and **21** were included in the guest panel in hopes of observing a mixture of the two possible diastereomeric complexes ((M)-**M3•20** and (P)-**M3•20**; (M)-**M3•21** and (P)-**M3•21**) arising due to the helical chirality of **M3**. Unfortunately, guests **20** and **21** do not display slow kinetics of guest exchange on the chemical shift time scale that is required to observe the diastereomeric complexes by ^{1}H NMR spectroscopy. Other guests that display slow kinetics of exchange in their complexation with **M3** include **1** and **13**. (Figure S30 & S42). Intermediate kinetics of exchange are observed for the complexes between **M3** and **2**, **3**, **6**, **11**, and **12**.

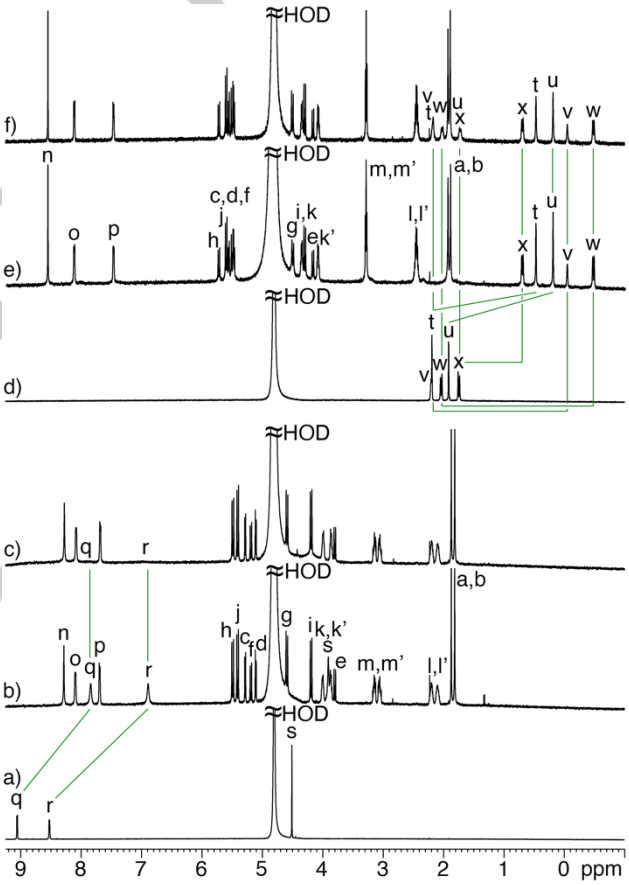

Figure 5. ^{1}H NMR spectra recorded (600 MHz, RT, D_2O) for: a) **14** (0.4 mM), b) an equimolar mixture of **M3** and **14** (0.2 mM), c) a mixture of **14** (0.4 mM) and **M3** (0.2 mM), d) **23** (0.4 mM), e) an equimolar mixture of **M3** and **23** (0.2 mM), and f) a mixture of **23** (0.4 mM) and **M3** (0.2 mM).

Measurement of the thermodynamic parameters of complex formation via ITC. After qualitatively analyzing the host•guest binding preferences of **M3**, we decided to gain insight into the thermodynamics of complexation. For this purpose, we turned to direct and competitive ITC measurements because the K_a values for acyclic CB[n]•guest complexes typically exceed the range accessible by ^{1}H NMR titrations (e.g. K_a > 10^4 M^{-1}). In addition, ITC directly provides the enthalpy of complexation (ΔH) and the

stoichiometry of binding. To assess the impact of the linear extension of aromatic sidewall from **M2** to **M3**, we first decided to measure the thermodynamic parameters of complexation between **M2** and a panel of typical (di)cationic guests (**1** – **24**) for CB[n]-type receptors (Table 1 and Figures S58 – S74). The K_a values for the **M2•1** – **M2•24** complexes range from (1.02 ± 0.02) × 10^6 (M^{-1}) for **M2•2** to (1.33 ± 0.23) × 10^{10} (M^{-1}) for **M2•24**. The **M2** complexes are uniformly driven by favorable enthalpic changes which is in accord with the known presence of high energy H_2O molecules in the cavity of CB[n]-type receptors that are released upon complexation.[33] Expectedly, the use of ITC to measure the binding of guests by **M3** was more difficult given that **M3** undergoes significant self-association (Figure 2) at room temperature and the determination of the **M3**•guest binding constants required additional precautions. Accordingly, we first conducted ITC experiments between **M3** and weak binding guest **26** at elevated temperatures (35 – 55 ˚C) where the effects of self-association of **M3** are minimized to determine K_a and ΔH as a function of temperature. A standard van't Hoff analysis allowed extrapolation of the K_a and ΔH values for **M3•26** to obtain values at 298 K (Figure S102). Subsequently, we performed competition ITC experiments with **26** as competitor to measure the thermodynamic parameters of binding for **M3**•guests that were both slightly tighter than **M3•26** and had significantly different ΔH values to provide sufficient heat upon guest exchange.[41] For the tighter **M3**•guest complexes and those with ΔH values similar to that of **M3•26** different competitors were selected. For example, Figure 6a shows the thermogram recorded for the competitive titration of a solution of **M3** (100 μM) and **4** (500 μM) in the cell with **24** (1.03 mM) in the syringe. Figure 6b shows the fitting of the integrated heat values to a 1:1 competitive binding model to extract K_a = (2.63 ± 0.1) × 10^{10} M^{-1} and ΔH = (-17.3 ± 0.02) kcal mol^{-1}. The K_a and ΔH values for the remaining **M3**•guest complexes are given in Table 1 and the data is presented in the Supporting Information (Figure S75 – S106). This dataset allows a dissection of the structure–binding constant relationships as described below.

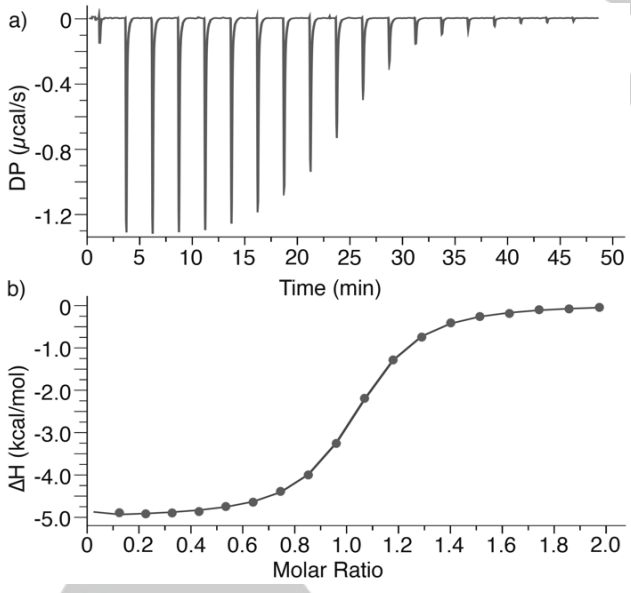

Figure 6. (a) Plot of change in DP vs time from the titration of **M3** (100 μM) and **4** (500 μM) in the cell with guest **24** (1.03 mM) in the syringe in 20 mM NaH_2PO_4 buffer (pH = 7.4); (b) plot of ΔH as a function of molar ratio of **M3** to **24**. The solid line represents the best non-linear fit of the data to the single set of sites model (K_a = (2.63 ± 0.10) × 10^{10} M^{-1} and ΔH = (-17.3 ± 0.02) kcal•mol^{-1}).

Table 1. Thermodynamic parameters (K_a (M^{-1}), ΔH˚ (kcal/mol) determined for the **M2**•guest and **M3**•guest complexes by ITC. Conditions: 298 K, 20 mM NaH_2PO_4 buffered H_2O, pH = 7.4.

Guest	**M2** K_a (M^{-1}) ΔH˚ (kcal/mol)	**M3** K_a (M^{-1}) ΔH˚ (kcal/mol)
1	(7.19 ± 0.19) × $10^{6[d]}$ (-7.36 ± 0.02)	(1.94 ± 0.1) × $10^{8[f]}$ (-10.8 ± 0.04)
2	(1.02 ± 0.02) × $10^{6[c]}$ (-9.40 ± 0.01)	(2.72 ± 0.2) × $10^{8[f]}$ (-11.4 ± 0.05)
3	(1.59 ± 0.06) × $10^{8[c]}$ (-8.23± 0.01)	(4.22 ± 0.3) × $10^{8[f]}$ (-12.1 ± 0.05)
4	(5.59 ± 0.17) × $10^{7[c]}$ (-9.70 ± 0.02)	(8.33 ± 0.9) × $10^{7[f]}$ (-12.2 ± 0.1)
5	(1.55 ± 0.04) × $10^{8[c]}$ (-9.84 ± 0.02)	(1.79 ± 0.2) × $10^{8[f]}$ (-13.0 ± 0.17)
6	(4.59 ± 0.09) × $10^{8[c][j]}$ (-10.6 ± 0.15)	(7.63 ± 1.0) × $10^{8[f]}$ (-14.2 ± 0.12)
7	(1.69 ± 0.11) × $10^{7[c]}$ (-8.96 ± 0.05)	(6.58 ± 0.4) × $10^{7[f]}$ (-13.6 ± 0.07)
8	(6.06 ± 0.18) × $10^{6[a]}$ (-9.86 ± 0.02)	(8.77 ± 0.4) × $10^{7[f]}$ (-13.1 ± 0.05)
9	(7.04 ± 0.24) × $10^{8[c]}$ (-10.9 ± 0.02)	(2.15 ± 0.3) × $10^{9[g]}$ (-14.1 ± 0.07)
10	(1.77 ± 0.09) × $10^{6[a]}$ (-5.54± 0.03)	(1.67 ± 0.1) × $10^{6[e]}$ (-7.29 ± 0.05)
11	(3.00 ± 0.07) × $10^{9[c][j]}$ (-13.3 ± 0.02)	(3.75 ± 0.1) × $10^{9[h]}$ (-16.1 ± 0.01)
12	(2.05 ± 0.12) × $10^{8[c]}$ (-11.6 ± 0.08)	Insoluble Complex
13	(2.53 ± 0.12) × $10^{9[c][j]}$ (-14.3 ± 0.04)	(1.45 ± 0.1) × $10^{10[i]}$ (-17.4 ± 0.05)
14	(2.14 ± 0.09) × $10^{9[c][j]}$ (-13.9 ± 0.04)	(4.26 ± 0.2) × $10^{9[h]}$ (-17.2 ± 0.06)
15	(2.92 ± 0.09) × $10^{7[c]}$ (-6.74 ± 0.03)	(7.63 ± 0.1) × $10^{6[e]}$ (-5.73 ± 0.04)
16	(7.09 ± 0.21) × $10^{8[c][j]}$ (-11.5 ± 0.02)	(2.87 ± 0.1) × $10^{8[f]}$ (-11.0 ± 0.03)
17	(6.54 ± 0.09) × $10^{6[e]}$ (-7.31 ± 0.01)	(1.49 ± 0.1) × $10^{7[f]}$ (-8.96 ± 0.09)
18	(1.88 ± 0.04) × $10^{7[e]}$ (-8.51 ± 0.01)	(3.23 ± 0.1) × $10^{7[f]}$ (-10.6 ± 0.04)
19	(3.15 ± 0.08) × $10^{6[a]}$ (-8.11 ± 0.02)	(3.76 ± 0.2) × $10^{8[f]}$ (-10.8 ± 0.03)
20	(1.96 ± 0.04) × $10^{8[c]}$ (-11.4 ± 0.02)	(1.24 ± 0.1) × $10^{9[f]}$ (-11.3 ± 0.02)
21	(2.68 ± 0.35) × $10^{8[c]}$ (-13.2 ± 0.15)	(4.48 ± 0.6) × $10^{8[f]}$ (-15.4 ± 0.16)
23	(2.87 ± 0.20) ×$10^{6[e]}$ (-4.32 ± 0.10)	(3.22 ± 0.4) × $10^{8[f]}$ (-8.33 ± 0.03)
24	(1.33 ± 0.23) × $10^{10[c][j]}$ (-15.2 ± 0.15)	(2.63 ± 0.1) × $10^{10[h]}$ (-17.3 ± 0.02)
26	n.d.	6.31 × $10^{5[b]}$ -6.51

[a] Direct ITC titration, [b] Direct ITC titration at elevated temperature by van't Hoff analysis, [c] measured by competitive ITC titration with **10**, [d] **13**, [e] **6**, [f] **26**, [g] **1**, [h] **4**, and [i] **16**. [j] Literature values.[39]

Discussion of the Trends in the Thermodynamic Parameters of Binding. The data in Table 1 shows that **M3** displays high affinity toward the panel of (di)cationic guests (**1**–**21**, **23**, **24**, **26**) with K_a values from 6.31 x 10^5 M^{-1} (**M3•26**) to 2.63 x 10^{10} M^{-1} (for **M3•24**). The Supporting Information (Figure S10) presents a bar graph comparing the binding affinity of **M1**, **M2**, and **M3** toward the guest panel. The **M3**•guest complexes are uniformly driven by favorable enthalpic changes as is common for CB[n]-type receptors.[33] The K_a values for a given guest toward **M3** are generally larger than those toward **M2** and **M1**. Given that **M2**

has already been used as an *in vivo* sequestration agent for neuromuscular blockers and drugs of abuse,[26a, b] the availability of the higher affinity **M3** variant may result in improved *in vivo* performance. Below, we analyze some of the trends in binding affinity as a function of guest structure that show that **M3** retains the essential binding characteristics of macrocyclic CB[n].

Influence of Guest Length. The length of the carbon linker between ammonium ions of diammonium ion guests (e.g. **4** – **6**) has been shown to have a significant effect on binding affinity toward CB[n] type receptors.[42] Guests with five or six carbon atom spacing between N-atoms have been found to display highest affinity due to a matching of the N•••N distance with the separation between the two electrostatically negative portals of CB[n]-type receptors. For hosts **M2** and **M3**, we observe a similar trend despite their ability to undergo out-of-plane skewing with K_a values increasing from **4** to **5** to **6**. Hosts **M3** and **M2** bind **6** significantly stronger than **4** (**M3**: 9.1-fold; **M2**: 8.2-fold).

Influence of Guest charge. It is known that each ammonium ion contributes significantly (up to 10^3) to CB[n]•guest binding affinity due to ion-dipole interactions.[33c, 42] As such, we selected two pairs of guests (**6** and **7**; **8** and **9**) that feature a common central hydrophobic binding domain and either one or two cationic N-atoms to assess their importance for acyclic CB[n]-type receptors **M2** and **M3**. We find that **M3** (**M2**) binds diammonium ions **6** 11.6-fold (27.1-fold) and **9** 24.5-fold (116-fold) tighter than monoammonium ions **7** and **8**. The 10 – 100-fold preference for the diammonium ions displayed by **M2** and **M3** is somewhat less than observed for CB[n] and suggests that the conformational flexibility of **M2** and **M3** and the presence of anionic SO_3^- solubilizing groups may make the ammonium ion binding site more diffuse.

Influence of guest methylation state and headgroup identity. It is known that increasing the methylation state of ammonium ions can increase the binding affinity toward CB[n] receptors, although the magnitude is quite guest dependent. The quaternary ammonium ions are thought to more uniformly spread the positive charge of the ammonium ion to the ureidyl C=O portals enhancing electrostatic contributions to binding free energy or increasing the hydrophobicity of the guest. As part of our guest panel, we selected **1** – **3**, and **6** that feature primary – quaternary hexanediammonium ion binding domains. Table 1 reveals that the binding affinity of **M3** toward guests **1** – **3** and **6** increases monotonically as the methylation state increases with a 3.9-fold difference between **M3•1** and **M3•6**. Host **M2** displayed a non-monotonic trend, but larger differences in affinity (63.8-fold) between **M2•1** and **M2•6**. Within our guest panel, other comparisons can be made between analogous pairs of primary and quaternary ammonium ion guests (**10** and **11**; **12** and **13**; **15** and **16**). Similarly, we find a preference for the quaternary over the primary ammonium ion guest (**M3**: **10**/**11** 2245-fold; **15**/**16** 37.6-fold; **M2**: **10**/**11** 1694-fold; **12**/**13** 12.3-fold; **15**/**16** 24.3-fold). Finally, we can make a comparison between **6** and **9** that differ in the nature of the headgroup (quaternary ammonium versus pyridinium). We find that **M3** and **M2** bind pyridinium ion **9** slightly stronger than **6** (**M3**: 2.81-fold; **M2**: 1.53-fold).

Influence of carbon number, size, and width of the guest hydrophobic moiety. An examination of Table 1 reveals that the number of carbon atoms in the hydrophobic moiety of the guest has a direct influence on guest affinity. For example, the cycloalkyl ammonium ions **17** (C7), **18** (C8), **19** (C12) show increased affinity toward **M3** as the number of carbons and the size of the guest increases; **M3** binds **19** 25.2-fold tighter than **18**. Interestingly, **M2** binds most tightly to **18** (6.0-fold selective over **19**) probably because the size of the cyclododecyl ring begins to exceed the size of the uncomplexed **M2** cavity. A related trend can be seen in the binding behavior of **6** (C6) and **24** (C10) which both contain a six-carbon spacing between N-atoms. **M3** (**M2**) displays higher affinity toward **24** than **6** (**M3**: 34.5-fold; **M2**: 29.0-fold). A consideration of the homologous series of guests (**6**, **13**, **11**, **14**, and finally **23**) that contain hydrophobic moieties of different size and width is also instructive. Across this series, **M3** is a more potent host than **M2** (**6**: 1.7-fold; **13**: 5.7-fold; **11**: 1.25-fold; **14**: 2.0-fold; **23**: 112-fold) and the selectivity becomes higher as the size / width of the guest exceeds the volume of the smaller **M2** hosts cavity. CB[8] was previously observed to bind **23** much stronger than CB[7] due to a more pronounced cavity size mismatch.[40] Overall, we conclude that **M3** retains the essential features of CB[n]-type receptors and that linear extension of the aromatic sidewalls from **M1** to **M2** to **M3** enhances binding affinity.

Binding towards Neuromuscular Blocking Agents (NMBA). Previously, we have investigated the use of **M1** and **M2** as *in vivo* reversal agents for the neuromuscular blocking agents rocuronium (roc, **27**), vecuronium (vec, **28**), and cisatracurium (cis, **25**).[26a, 26c, 43] In these applications, the abiotic receptor competes directly with the biological receptor and lowers NMBA concentration by a pharmacokinetic strategy. It is important that new reversal agents for NMBAs display high affinity to the neuromuscular blockers, but discriminate against acetylcholine (ACh, **22**) which is also present in the neuromuscular junction. Accordingly, we measured the binding constants of **M3** toward **22**, **25**, and **27** – **29** by ITC (Table 2). The dissociation constants for the **M3•27** – **M3•29** are in the low pM range. Significantly, **M3** displays higher affinity than **M2** toward **25** (69-fold), **27** (7.4-fold), **28** (11.2-fold), and **29** (25-fold). Equally importantly, **M3** only binds 2.8-fold tighter to ACh **22** than **M2**. High selectivity for the NMBA versus ACh is crucial to the *in vivo* function of the reversal agent. Accordingly, **M3** holds promise as a next generation agent for *in vivo* reversal of neuromuscular block.

Table 2. Thermodynamic parameters (K_a (M^{-1}), ΔH° (kcal/mol) determined for the **M2**•NMBA and **M3**•NMBA complexes by ITC. Conditions: 298 K, 20 mM NaH_2PO_4 buffered H_2O, pH = 7.4.

Guest	**M2** K_a (M^{-1}) ΔH° (kcal/mol)	**M3** K_a (M^{-1}) ΔH° (kcal/mol)
22	$(1.79 \pm 0.05) \times 10^{5[d]}$ (-7.27 ± 0.04)	$(5.0 \pm 0.2) \times 10^{5[b]}$ (-10.7 ± 0.03)
25	$(1.28 \pm 0.18) \times 10^{5[d]}$ (-13.3 ± 0.793)	$(8.85 \pm 0.72) \times 10^{6[c]}$ (-14.4 ± 0.16)
27	$(5.78 \pm 2.68) \times 10^{9[d]}$ (-13.5 ± 0.03)	$(4.3 \pm 0.1) \times 10^{10[a]}$ (-17.2 ± 0.03)
28	$(4.02 \pm 0.32) \times 10^{9[d]}$ (-9.33 ± 0.03)	$(4.5 \pm 0.8) \times 10^{10[a]}$ (-13.1 ± 0.03)

29	$(8.0 \pm 0.69) \times 10^{8}$[d] (-9.33 ± 0.03)	$(2.0 \pm 0.1) \times 10^{10}$[a] (-12.6 ± 0.03)

Measured by competitive ITC titration with: [a] **23**, [b] **6**, [c] **26**. [d] Reported in the literature.[43b]

Fluorescence Sensing Array Based on M3. Given the change in angle, orientation, and potentially helicity of the two anthracene chromophores upon guest binding as shown by x-ray crystallography and the brighter chromophore of **M3** relative to **M2** and analogues[27] lead us to consider if **M3** would function as a versatile component of sensing arrays.[13b, 44] As a proof-of-concept, we used the fluorescence response of **M3** (Figure 8) to discriminate among the very similar members of our guest panel. Experimentally, we used a 96-well plate format to excite **M3** at 260 nm and measure the fluorescence of **M3** (2.0 μM, 5.0 μM, 10.0 μM) alone and when mixed guests **1** – **21**, **23**, **24**, and **26** (5.0 μM). The fluorescence intensities were extracted from the spectra (every 5 nm from 415 to 460 nm) to create the dataset used as input for the dimensionality reduction and classification method linear discriminant analysis (LDA).[45] Because the fluorescence intensity depends on not only concentrations and binding constants, but also on complex geometry (e.g. chromophore orientation) and guest structure, the dataset is information rich. Accordingly, we used LDA to find new variables that more efficiently explained the data by using a linear combination of the measured spectral intensities (Figure 7). Classification of the analytes by LDA using only the first two linear discriminants (LD) was found to be 91 ± 2 % accurate after randomly splitting the data into 10 sections and using k-fold cross validation. Given the structural similarity between members of the guest panel, we find such levels of discrimination to be encouraging. For example, the array distinguishes efficiently based on the degree of alkylation of ammonium ions (e.g. **1** – **3** and **6**; **10** and **11**; **12** and **13**; **15** and **16**) presumably due in part to differences in **M3**•guest K_a. Discrimination between diammonium guests with different hydrophobic moieties (e.g. **6**, **11**, **13**, **14**, **23**) is also efficient. One subset of guests that cannot be discriminated are compounds **8**, **9**, and **14** which contain electronic deficient pyridinium units which fully quench and therefore eliminate the difference in fluorescence of those **M3**•guest complexes. It is worth emphasizing that the LDA plots were created using a single host (**M3**) at only 3 concentrations. We believe that sensing arrays comprising **M3**, other hosts, and auxiliary chromophores will greatly extend the range of sensing applications that can be tackled. Finally, the observed helical chirality of **M3** suggests that circular dichroism will be a powerful method to distinguish between chiral analytes and determine enantiomeric excess values.[13b, 23b, 46]

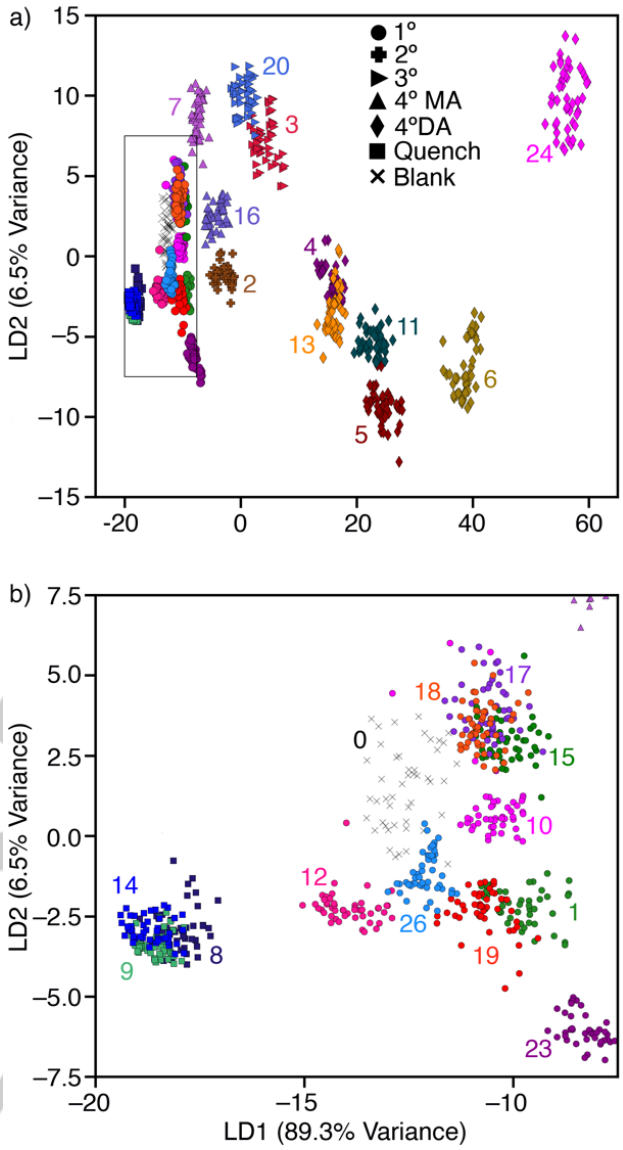

Figure 7. a) LDA plot of the first two linear discriminants (95.8% of overall variance) showing the separation and classification of analytes **1**–**20**, **23**, **24**. b) Expanded region from the grey boxed area of panel a). Three different concentrations of **M3** (2.0 μM, 5.0 μM, and 10.0 μM) were mixed with 5 μM analyte in separate wells of a 96-well plate and analyzed for changes in fluorescence across each spectrum (415 nm – 460 nm at intervals of every 5 nm.

Conclusion

In summary, we have reported the linear extension of the aromatic sidewalls of acyclic CB[n]-type containers from benzene to naphthalene to anthracene in the form of **M3**. We find that **M3** is nicely soluble in aqueous solution (≈ 30 mM) but does undergo noticeable self-association in water. X-ray crystallography (Figure 3) shows that linear extension of the aromatic sidewalls forces **M3** and the **M3**•**20** complex to assume a helical conformation to alleviate steric interactions between the sidewalls. ^{1}H NMR studies indicates fast kinetics of guest exchange and host helicity inversion for most **M3**•guest complexes, but one of the largest guests (**23**) displays slow exchange kinetics. The thermodynamics of binding for the **M2**•guest and **M3**•guest

complexes were determined by ITC and found to be uniformly driven by favorable enthalpic changes. We find that **M3** with its extended aromatic walls generally exhibits higher binding constants towards the panel of guests. Of particular interest is the enhanced binding affinities displayed by **M3** toward the neuromuscular blockers roc, vec, and cis compared to **M2** which functions as an *in vivo* reversal agent for this important class of drugs. Finally, the enhanced optical properties of anthracene walled **M3** and the dependence of fluorescence intensity upon anthracene-anthracene orientation (e.g. **M3**•guest geometry), guest structure, and binding constants renders **M3** a powerful component of sensing arrays. In conclusion, the work shows that linear π-extension of the aromatic sidewalls endows **M3** with enhanced binding affinity toward cationic guests including clinically important neuromuscular blockers, enhances their optical characteristics, and results in helically chirality. As such, **M3** and analogues possess great potential as *in vivo* reversal agents and as components of sensing arrays for the analysis of achiral and chiral analytes.

Acknowledgements

We thank the National Science Foundation (CHE-1807486) and the National Institutes of Health (GM132345) for financial support. S.M. thanks the University of Maryland for a Department of Education GAANN (P200A150033) fellowship and an Ann G. Wylie Dissertation fellowship. We thank Prof. Kata Mlinaric-Majerski and Prof. Marina Sekutor for supplying guest **23**.

Keywords: cucurbituril • neuromuscular blockers • fluorescence sensing • molecular recognition • helical chirality

[1] a) D. J. Cram, *Angew. Chem. Int. Ed.* **1988**, *27*, 1009-1020; b) J.-M. Lehn, *Angew. Chem., Int. Ed. Engl.* **1988**, *27*, 89-112; c) C. J. Pedersen, *Angew. Chem., Int. Ed. Engl.* **1988**, *27*, 1021-1027.

[2] a) E. V. Anslyn, *J. Org. Chem.* **2007**, *72*, 687-699; b) B. Daly, T. S. Moody, A. J. M. Huxley, C. Yao, B. Schazmann, A. Alves-Areias, J. F. Malone, H. Q. N. Gunaratne, P. Nockemann, A. P. de Silva, *Nat. Commun.* **2019**, *10*, 1-7.

[3] a) J. F. Stoddart, *Angew. Chem. Int. Ed.* **2017**, *56*, 11094-11125; b) B. L. Feringa, *Angew. Chem., Int. Ed.* **2017**, *56*, 11060-11078; c) J.-P. Sauvage, *Angew. Chem., Int. Ed.* **2017**, *56*, 11080-11093.

[4] T. F. A. De Greef, M. M. J. Smulders, M. Wolffs, A. P. H. J. Schenning, R. P. Sijbesma, E. W. Meijer, *Chem. Rev.* **2009**, *109*, 5687-5754.

[5] W. H. Pirkle, C. J. Welch, *Tetrahedron Asymmetry* **1994**, *5*, 777-780.

[6] V. J. Stella, V. M. Rao, E. A. Zannou, V. Zia, *Adv. Drug Delivery Rev.* **1999**, *36*, 3-16.

[7] C. D. Gutsche, *Acc. Chem. Res.* **1983**, *16*, 161-170.

[8] F. Diederich, *Angew. Chem., Intl. Ed. Engl.* **1988**, *27*, 362-386.

[9] a) R. Pinalli, E. Dalcanale, *Acc. Chem. Res.* **2013**, *46*, 399-411; b) Y. Yu, J. Rebek, *Acc. Chem. Res.* **2018**, *51*, 3031-3040; c) J. H. Jordan, B. C. Gibb, *Chem. Soc. Rev.* **2015**, *44*, 547-585.

[10] a) T. Ogoshi, T.-A. Yamagishi, Y. Nakamoto, *Chem. Rev.* **2016**, *116*, 7937-8002; b) M. Xue, Y. Yang, X. Chi, Z. Zhang, F. Huang, *Acc. Chem. Res.* **2012**, *45*, 1294-1308; c) J.-R. Wu, Y.-W. Yang, *Chem. Commun.* **2019**, *55*, 1533-1543.

[11] a) K. Harris, D. Fujita, M. Fujita, *Chem. Commun.* **2013**, *49*, 6703-6712; b) J. Rebek, *Acc. Chem. Res.* **2009**, *42*, 1660-1668; c) S. Zarra, D. M. Wood, D. A. Roberts, J. R. Nitschke, *Chem. Soc. Rev.* **2015**, *44*, 419-432.

[12] Febreze Home Page. https://www.febreze.com/en-us (accessed May 5, 2020).

[13] a) R. A. Tromans, T. S. Carter, L. Chabanne, M. P. Crump, H. Li, J. V. Matlock, M. G. Orchard, A. P. Davis, *Nat. Chem.* **2019**, *11*, 52-56; b) M. K. Meadows, E. V. Anslyn, *Macrocyclic Supramol. Chem.* **2016**, 92-126.

[14] B. A. Moyer, R. Custelcean, B. P. Hay, J. L. Sessler, K. Bowman-James, V. W. Day, S.-O. Kang, *Inorg. Chem.* **2013**, *52*, 3473-3490.

[15] M. J. Klemes, Y. Ling, C. Ching, C. Wu, L. Xiao, D. E. Helbling, W. R. Dichtel, *Angew. Chem., Int. Ed.* **2019**, *58*, 12049-12053.

[16] a) K. M. Park, J. Murray, K. Kim, *Acc. Chem. Res.* **2017**, *50*, 644-646; b) E. Masson, X. Ling, R. Joseph, L. Kyeremeh-Mensah, X. Lu, *RSC Adv.* **2012**, *2*, 1213-1247; c) K. I. Assaf, W. M. Nau, *Chem. Soc. Rev.* **2015**, *44*, 394-418; d) S. J. Barrow, S. Kasera, M. J. Rowland, J. del Barrio, O. A. Scherman, *Chem. Rev.* **2015**, *115*, 12320-12406.

[17] a) D. Shetty, J. K. Khedkar, K. M. Park, K. Kim, *Chem. Soc. Rev.* **2015**, *44*, 8747-8761; b) L. Cao, M. Sekutor, P. Y. Zavalij, K. Mlinaric-Majerski, R. Glaser, L. Isaacs, *Angew. Chem. Int. Ed.* **2014**, *53*, 988-993.

[18] R. Dsouza, A. Hennig, W. Nau, *Chem. Eur. J.* **2012**, *18*, 3444-3459.

[19] Y. H. Ko, E. Kim, I. Hwang, K. Kim, *Chem. Commun.* **2007**, 1305-1315.

[20] H. Yin, R. Wang, *Isr. J. Chem.* **2017**, *58*, 188-198.

[21] A. Palma, M. Artelsmair, G. Wu, X. Lu, S. J. Barrow, N. Uddin, E. Rosta, E. Masson, O. A. Scherman, *Angew. Chem., Int. Ed.* **2017**, *56*, 15688-15692.

[22] Aqdot Home Page. https://aqdot.com (accessed May 6, 2020).

[23] a) S. Ganapati, L. Isaacs, *Isr. J. Chem.* **2018**, *58*, 250-263; b) A. Prabodh, D. Bauer, S. Kubik, P. Rebmann, F. G. Klaerner, T. Schrader, L. Delarue Bizzini, M. Mayor, F. Biedermann, *Chem. Commun.* **2020**, *56*, 4652-4655; c) D. Mao, Y. Liang, Y. Liu, X. Zhou, J. Ma, B. Jiang, J. Liu, D. Ma, *Angew. Chem. Int. Ed.* **2017**, *41*, 12614-12618.

[24] a) F.-G. Klaerner, T. Schrader, *Acc. Chem. Res.* **2013**, *46*, 967-978; b) K. Jono, A. Suzuki, M. Akita, K. Albrecht, K. Yamamoto, M. Yoshizawa, *Angew. Chem., Int. Ed.* **2017**, *56*, 3570-3574.

[25] G. Hettiarachchi, S. K. Samanta, S. Falcinelli, B. Zhang, D. Moncelet, L. Isaacs, V. Briken, *Mol. Pharmaceutics* **2016**, *13*, 809-818.

[26] a) F. Haerter, J. C. P. Simons, U. Foerster, I. Moreno Duarte, D. Diaz-Gil, S. Ganapati, K. Eikermann-Haerter, C. Ayata, B. Zhang, M. Blobner, L. Isaacs, M. Eikermann, *Anesthesiology* **2015**, *123*, 1337-1349; b) S. Ganapati, S. D. Grabitz, S. Murkli, F. Scheffenbichler, M. I. Rudolph, P. Y. Zavalij, M. Eikermann, L. Isaacs, *ChemBioChem* **2017**, *18*, 1583-1588; c) D. Ma, B. Zhang, U. Hoffmann, M. G. Sundrup, M. Eikermann, L. Isaacs, *Angew Chem Int Ed Engl* **2012**, *51*, 11358-11362.

[27] a) T. Minami, N. A. Esipenko, B. Zhang, L. Isaacs, R. Nishiyabu, Y. Kubo, P. Anzenbacher, *J. Am. Chem. Soc.* **2012**, *134*, 20021-20024; b) T. Minami, N. A. Esipenko, A. Akdeniz, B. Zhang, L. Isaacs, P. Anzenbacher, *J. Am. Chem. Soc.* **2013**, *135*, 15238-15243; c) E. G. Shcherbakova, B. Zhang, S. Gozem, T. Minami, Y. Zavalij Peter, M. Pushina, L. Isaacs, P. J. Anzenbacher, *J. Am. Chem. Soc.* **2017**, *139*, 14954-14960.

[28] L. Gilberg, B. Zhang, P. Y. Zavalij, V. Sindelar, L. Isaacs, *Org. Biomol. Chem.* **2015**, *13*, 4041-4050.

[29] a) B. Zhang, P. Y. Zavalij, L. Isaacs, *Org. Biomol. Chem.* **2014**, *12*, 2413-2422; b) D. Sigwalt, D. Moncelet, S. Falcinelli, V. Mandadapu, P. Y. Zavalij, A. Day, V. Briken, L. Isaacs, *ChemMedChem* **2016**, *11*, 980-989.

[30] S. Ganapati, L. Isaacs, *Supramol. Chem.* **2019**, *31*, 114-126.

[31] B. Zhang, L. Isaacs, *J. Med. Chem.* **2014**, *57*, 9554-9563.

[32] X. Lu, S. K. Samanta, P. Y. Zavalij, L. Isaacs, *Angew. Chem., Int. Ed.* **2018**, *57*, 8073-8078.

[33] a) F. Biedermann, V. D. Uzunova, O. A. Scherman, W. M. Nau, A. De Simone, *J. Am. Chem. Soc.* **2012**, *134*, 15318-15323; b) F. Biedermann, W. M. Nau, H.-J. Schneider, *Angew. Chem. Int. Ed.* **2014**, *53*, 11158-11171; c) W. M.

Nau, M. Florea, K. I. Assaf, *Isr. J. Chem.* **2011**, *51*, 559-577.
[34] a) Y. Hong, J. Chen, Z. Zhang, Y. Liu, W. Zhang, *Org. Lett.* **2016**, *18*, 2640-2643; b) Z. Chen, J. P. Amara, J. P. Thomas, T. M. Swager, *Macromolecules* **2006**, *39*, 3202-3209.
[35] S. Z. Ndendjio, W. Liu, N. Yvanez, Z. Meng, P. Y. Zavalij, L. Isaacs, *New J. Chem.* **2020**, *44*, 338-345.
[36] S. Ghosh, A. Wu, J. C. Fettinger, P. Y. Zavalij, L. Isaacs, *J. Org. Chem.* **2008**, *73*, 5915-5925.
[37] M. Nishio, *CrystEngComm* **2004**, *6*, 130-158.
[38] W. Boczon, *J. Mol. Structure* **1987**, *158*, 127-139.
[39] K. G. Brady, L. Gilberg, D. Sigwalt, J. Bistany-Riebman, S. Murkli, J. Klemm, P. Kulhánek, P. Šindelář, *Supramol. Chem.* **2020**, DOI: 10.1080/10610278.2020.1795173
[40] D. Sigwalt, M. Sekutor, L. Cao, P. Y. Zavalij, J. Hostas, H. Ajani, P. Hobza, K. Mlinaric-Majerski, R. Glaser, L. Isaacs, *J. Am. Chem. Soc.* **2017**, *139*, 3249-3258.
[41] a) T. Wiseman, S. Williston, J. F. Brandts, L.-N. Lin, *Anal. Biochem.* **1989**, *179*, 131-137; b) J. Broecker, C. Vargas, S. Keller, *Anal. Biochem.* **2011**, *418*, 307-309.
[42] W. L. Mock, N.-Y. Shih, *J. Org. Chem.* **1986**, *51*, 4440-4446.
[43] a) U. Hoffmann, M. Grosse-Sundrup, K. Eikermann-Haerter, S. Zaremba, C. Ayata, B. Zhang, D. Ma, L. Isaacs, M. Eikermann, *Anesthesiology* **2013**, *119*, 317-325; b) D. Shaya, L. Isaacs, *Croat. Chem. Acta* **2019**, *92*, 163-171.
[44] a) Z. Li, J. R. Askim, K. S. Suslick, *Chem. Rev.* **2019**, *119*, 231-292; b) S. Sinn, E. Spuling, S. Brase, F. Biedermann, *Chem. Sci.* **2019**, *10*, 6584-6593.
[45] a) J. R. Lakowicz, *Principles of Fluorescence Spectroscopy*, 3rd ed., Springer, New York, **2006**; b) J. Miller, J. C. Miller, *Statistics and Chemometrics for Analytical Chemistry*, 6th ed., Pearson, Harlow, **2010**.
[46] Z. A. De los Santos, C. Wolf, *J. Am. Chem. Soc.* **2020**, *142*, 4121-4125.

WILEY-VCH

Entry for the Table of Contents

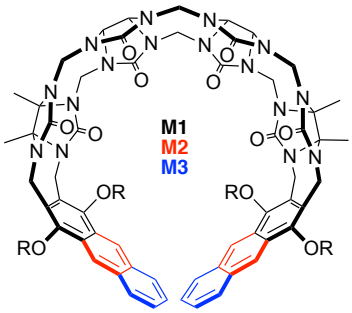

R = $(CH_2)_3SO_3Na$

Twist and Shout: Linear extension of the walls of acyclic CB[n]-type receptors from **M1** to **M2** to **M3** results in helical chirality. Anthracene walled **M3** displays superior binding affinity compared to **M1** and **M2** toward hydrophobic (di)cations including the clinically important neuromuscular blockers. The fluorescence output of **M3** is sensitive to sidewall orientation, guest identity and concentration, and K_a which renders **M3** a versatile component for sensing arrays.

@LyleIsaacsUMD, @MurkliSteven

WILEY-VCH